Mechanistic Investigations of the Asymmetric Hydrogenation of Enamides with Neutral Bis(phosphine) Cobalt Precatalysts

Lauren N. Mendelsohn,[a] Ljiljana Pavlovic,[b] Hongyu Zhong,[a] Max R. Friedfeld,[a] Michael Shevlin,[c] Kathrin H. Hopmann,[b*] Paul J. Chirik[a*]

[a]Department of Chemistry, Princeton University, New Jersey 08544, United States.

[b]Department of Chemistry, UiT The Arctic University of Norway, N-9037 Tromsø, Norway.

[c]Department of Process Research & Development, Merck & Co., Inc., Rahway, New Jersey 07065, United States.

Supporting Information Placeholder

ABSTRACT: The mechanism of the asymmetric hydrogenation of prochiral enamides by well defined, neutral bis(phosphine) cobalt(0) and cobalt(II) precatalysts has been explored using (*R*,*R*)-^{iPr}DuPhos ((*R*,*R*)-^{iPr}DuPhos = (+)-1,2-bis[(2*R*,5*R*)-2,5-diisopropylphospholano]benzene) as a representative chiral bis(phosphine) ligand. A series of (*R*,*R*)-(^{iPr}DuPhos)Co(enamide) (enamide = methyl-2-acetamidoacrylate (MAA), methyl(*Z*)-α-acetamidocinnamate (MAC), and methyl(*Z*)-acetamido(4-fluorophenyl)acrylate (^{4F}MAC)) complexes (**1-MAA**, **1-MAC**, **1-^{4F}MAC**), as well as a dinuclear cobalt tetrahydride, [(*R*,*R*)-(^{iPr}DuPhos)Co]$_2$(μ_2-H)$_3$(H) (**2**) were independently synthesized, characterized, and evaluated in both stoichiometric and catalytic hydrogenation reactions. Characterization of (*R*,*R*)-(^{iPr}DuPhos)Co(enamide) complexes by X-ray diffraction established the formation of the pro-(*R*) diastereomers in contrast to the (*S*)-alkane products obtained from the catalytic reaction. In-situ monitoring of the cobalt-catalyzed hydrogenation reactions by UV-visible and freeze-quench electron paramagnetic resonance (EPR) spectroscopies revealed (*R*,*R*)-(^{iPr}DuPhos)Co(enamide) complexes as the catalyst resting state for all three enamides studied. Variable time normalization analysis (VTNA) kinetic studies of the cobalt-catalyzed hydrogenation reactions in methanol established a rate law that is first-order in (*R*,*R*)-(^{iPr}DuPhos)Co(enamide) and H_2 but independent of the enamide concentration. Deuterium-labeling studies, including measurement of an H_2/D_2 kinetic isotope effect and catalytic hydrogenations with HD, established an irreversible H_2 addition step to the bound enamide. Density functional theory (DFT) calculations support that this step is both rate- and selectivity-determining. Calculations, as well as HD labeling studies, provide evidence for two-electron redox cycling involving cobalt(0) and cobalt(II) intermediates during the catalytic cycle. Taken together, these experiments support an unsaturated pathway for the [(*R*,*R*)-(^{iPr}DuPhos)Co]-catalyzed hydrogenation of prochiral enamides.

INTRODUCTION

Transition metal-catalyzed asymmetric hydrogenation of prochiral alkenes is one of the most widely used methods for the preparation of single enantiomer compounds.[1-4] Alongside well-established precious-metal rhodium, iridium, and ruthenium catalysts, chiral bis(phosphine) cobalt complexes have emerged as a privileged class of catalysts for this transformation, generating highly enantioenriched alkane products from a range of prochiral alkenes (Scheme 1a). Well-defined precatalysts have been prepared across a range of cobalt oxidation states, including neutral bis(phosphine) cobalt(0), (I), and (II),[5,6] as well as cationic bis(phosphine) cobalt(I) derivatives.[7] In-situ catalyst generation from a combination of bis(phosphine), readily available cobalt precursors, such as $CoCl_2$•$6H_2O$, and zinc enables a reliable method for catalyst discovery by high-throughput experimentation.[6] Bis(phosphine) cobalt catalysts have demonstrated remarkable activity and functional group tolerance and the highly enantioselective hydrogenation of unfunctionalized olefins,[5] enamides,[6] carboxylic acids,[8-10] hydrazones,[11] and enynes[12] have all been reported. Notable examples include the efficient hydrogenation of pharmaceutically-relevant substrates such as dehydro-levetiracetam and the precursor to L-DOPA.[6,8] In addition, bis(phosphine) cobalt complexes have been widely used for a host of catalytic C–C bond-forming reactions, including examples with high levels of enantioselectivity.[13-18]

While bis(phosphine)cobalt(0) complexes are expected to be highly reducing, these catalysts exhibit high and often optimal activity and enantioselectivity in methanol and other protic solvents.[6] Despite the synthetic utility and high enantioselectivity across a range of substrates, limited experimental evidence has been provided to understand the mechanism of action and origin of enantioselectivity with this class of catalysts. Open questions include: the resting state of the catalyst, the interaction of precatalysts with reactants (hydrogen and alkenes), the enantio- and rate-determining steps, and the role of cobalt redox cycling versus redox-neutral pathways.

Scheme 1. Mechanistic investigations of bis(phosphine) rhodium- and cobalt-catalyzed asymmetric enamide hydrogenation.

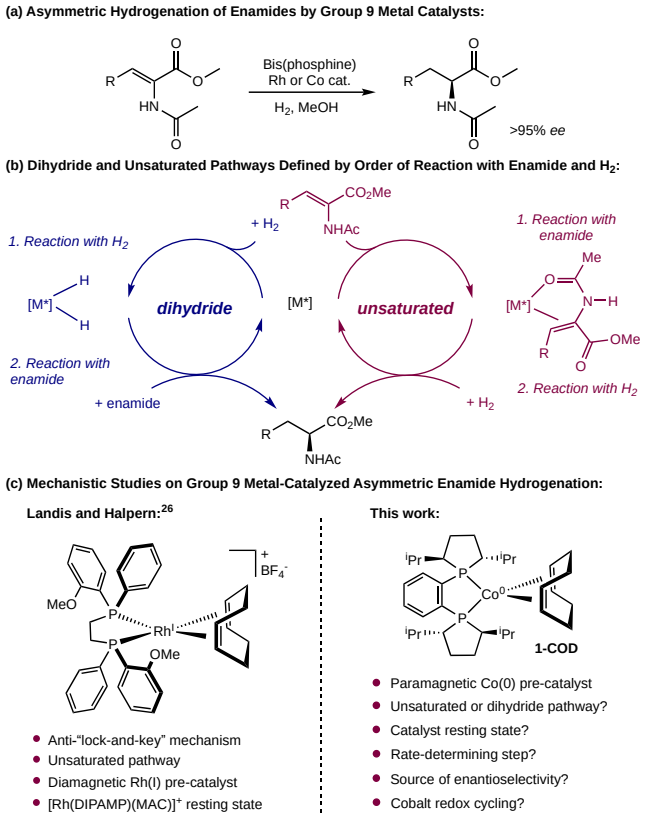

In contrast, the mechanism of the asymmetric hydrogenation of enamides with cationic bis(phosphine) rhodium(I) precatalysts has been extensively studied. Two major mechanistic pathways have been proposed, differentiated by the order of the reaction with respect to the reactants, enamide and hydrogen. In an unsaturated pathway, rhodium-enamide complex formation precedes the reaction with H_2 (Scheme 1b, right), whereas in a dihydride pathway, rhodium-dihydride complex formation precedes the reaction with the enamide (Scheme 1b, left). Both unsaturated and dihydride pathways have been experimentally supported, with mechanistic distinctions depending on the identity of the bis(phosphine) ligand and the enamide substrate being used.[19] In their landmark studies on the (DIPAMP)rhodium-catalyzed (DIPAMP = (*R*,*R*)-ethylenebis[(2-methoxyphenyl)phenylphosphine]) asymmetric hydrogenation of prochiral enamides, Landis and Halpern,[20-26] established an unsaturated anti-"lock-and-key" pathway, where rhodium-enamide diastereomers are rapidly equilibrating in solution and enantioselection is a result of their relative rates of hydrogen activation, rather than the relative abundance of the diastereomers in solution. Specifically, Landis and Halpern found a pathway that fit the "major-minor" concept, where the minor diastereomer of the rhodium-enamide resting state led to the major enantiomer of the product, with diastereomer interconversion facilitated by formation of methanol solvento complexes (Scheme 1c, left). In contrast, Gridnev, Imamoto and others studying rhodium(I) catalysts with more electron donating bis(phosphine) ligands have provided evidence for dihydride pathways.[27-36] Here it is proposed that enantioselection occurs after enamide association to the cobalt complex, through partial dissociation and reassociation of the C=C bond and enantio-determining migratory insertion. Work by Brown and coworkers identified intermediates relevant to both limiting mechanisms.[37-43]

The limited experimental mechanistic understanding for cobalt-catalyzed asymmetric hydrogenation inspired studies into the mechanism of the neutral bis(phosphine) cobalt-catalyzed asymmetric hydrogenation of prochiral enamides (Scheme 1c, right).[9-11] In comparison to the reported studies on cationic rhodium(I) catalysis, neutral cobalt(0/II) complexes are paramagnetic. The featureless ^{1}H NMR spectra and the absence of any observable ^{31}P NMR signals due to the paramagnetism complicated their characterizations. This is in contrast to the rhodium catalysts, where diagnostic sets of ^{31}P NMR signals with fine splitting patterns have enabled the straightforward differentiation of rhodium diastereomers and other intermediates in solution.[20–43] To overcome this challenge, we have turned to a combination of UV-visible and EPR spectroscopies, as well as X-ray crystallography and DFT studies to characterize well-defined cobalt complexes and reaction intermediates. Here we describe mechanistic studies on the neutral, [(*R*,*R*)-(^{iPr}DuPhos)Co]-catalyzed ((*R*,*R*)-^{iPr}DuPhos = (+)-1,2-bis[(2*R*,5*R*)-2,5-diisopropylphospholano]benzene) asymmetric hydrogenation of simple prochiral enamides. Through organometallic studies, kinetic analysis, deuterium labeling experiments, and DFT calculations, our studies support an unsaturated pathway for [(*R*,*R*)-(^{iPr}DuPhos)Co] complexes, with a cobalt-enamide resting state and a rate-determining oxidative hydride transfer from H_2 to the enamide. Both experimental and computational evidence support the possibility of cobalt-redox cycling.

RESULTS AND DISCUSSION

Synthesis, Characterization, and Evaluation of Bis(phosphine) Cobalt(0)-Enamide Complexes. Our studies commenced with evaluation of both unsaturated and dihydride pathways for bis(phosphine) cobalt-catalyzed asymmetric enamide hydrogenation. Key to each of these pathways is one of the following intermediates: bis(phosphine) cobalt-enamide and bis(phosphine) cobalt-dihydride complexes for the unsaturated and dihydride pathways, respectively. To evaluate an unsaturated pathway, the synthesis of bis(phosphine) cobalt-enamide complexes was targeted to determine the spectroscopic signatures, stability, and reactivity of these potential catalytic intermediates.

Our laboratory has reported that addition of 1 atm of H_2 to the cobalt dialkyl complex, (*R*,*R*)-(^{iPr}DuPhos)Co(CH_2SiMe_3)$_2$, in the presence of 1,5-cyclooctadiene (COD) resulted in isolation of the formally cobalt(0)-diene complex, (*R*,*R*)-(^{iPr}DuPhos)Co(COD) (**1-COD**).[6] This synthetic method was applied to the synthesis of (*R*,*R*)-(^{iPr}DuPhos)Co(enamide) complexes each bearing one of the three representative enamides used in this study: methyl 2-acetamidoacrylate (MAA), methyl(*Z*)-α-acetamidocinnamate (MAC), and methyl(*Z*)-acetamido(4-fluorophenyl)acrylate (^{4F}MAC). Addition of 1 atm of H_2 to a THF solution of (*R*,*R*)-(^{iPr}DuPhos)Co(CH_2SiMe_3)$_2$ in the presence of one equivalent of enamide resulted in a rapid color change from orange to dark red-brown, signaling the formation of the targeted cobalt-enamide complexes, (*R*,*R*)-(^{iPr}DuPhos)Co(MAA) (**1-MAA**, 93% yield), (*R*,*R*)-(^{iPr}DuPhos)Co(MAC) (**1-MAC**, 95% yield), (*R*,*R*)-(^{iPr}DuPhos)Co(^{4F}MAC) (**1-^{4F}MAC**, 91% yield) (Scheme 2). While this transformation occurs too rapidly to be thoroughly studied using routine spectroscopic techniques, it likely occurs through a two-electron reduction by either a bis(phosphine)cobalt-dihydride intermediate formed from the

hydrogenolysis of two methylene trimethylsilane groups or directly to the bis(phosphine) cobalt-enamide complex through the hydrogenolysis of a single methylene trimethylsilane group and subsequent C–H reductive elimination.

Scheme 2. General method for the synthesis of (*R*,*R*)-(^{iPr}DuPhos)Co(enamide) complexes.

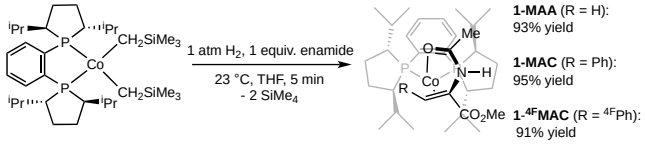

The solid-state structures of all three cobalt(enamide) complexes were determined by single-crystal X-ray diffraction (Figure 1) and established similar distorted square pyramidal geometries with two-point coordination of the substrate to cobalt at both the enamide oxygen and the C=C bond. Significant lengthening of the C=C bond was observed in all three structures (Table 1). For the square pyramidal, neutral cobalt(0) complexes, the alkene occupies the basal plane and the carbonyl oxygen occupies the axial position. By comparison, for the square-planar, cationic cobalt(I)[7] and rhodium(I)[24] complexes, both alkene and the carbonyl oxygen lie in the basal plane. This finding highlights the unique properties of asymmetric catalysis with cobalt(0) and cobalt(I) catalysts where stereo-interaction between the identical pro-chiral substrate and chiral ligand is altered by merely a one-electron redox event at cobalt. While the unit cell of **1-MAA** contained both the pro-(*R*) and pro-(*S*) diastereomers in a 1:1 ratio, the crystals of both **1-MAC** and **1-^{4F}MAC** contained only the pro-(*R*) diastereomer. Interestingly, this is the opposite stereochemistry from the (*S*)-enantiomer obtained from catalytic hydrogenation of all three enamides with **1-COD**. The paramagnetic benzene-d_6 ^{1}H NMR spectra exhibited broad, featureless resonances and accordingly, benzene-d_6 solution magnetic moments each corresponded to an S=1/2 ground state (Table 1).[44] The X-band EPR spectra for each complex in toluene or THF glass (10 K) exhibited a distinct rhombic signal consistent with an S = ½ cobalt complex exhibiting diagnostic hyperfine coupling of g_x tensor to the ^{59}Co nucleus (I = 7/2, 100% natural abundance) (Figure 2).

Table 1. Magnetic data and C=C bond distances observed in cobalt(enamide) complexes.

Complex	Magnetic Moment (μ_B)	C=C Bond Length (Å)
1-MAA	2.0(3)	pro-(*R*) 1.455(9) pro-(*S*) 1.398(9)
1-MAC	2.0(1)	1.44(2)
1-^{4F}MAC	1.8(1)	1.4668(9)

It is important to note that observation of a particular diastereomer in the solid-state structure is not necessarily a reflection of the diastereomeric ratio of the bulk sample. Due to the uninformative nature of the NMR spectra for these cobalt(enamide) complexes and their high solubility in hydrocarbon solvents, further information about solution-state diastereomeric ratios were not obtained. However, as will be discussed later in this text, density functional theory calculations (PBE0-D3BJ, [IEFPCM(methanol)] performed on **1-MAA** demonstrated only a 0.2 kcal/mol energy difference between the pro-(*R*) and pro-(*S*) diastereomers, supporting the hypothesis that they likely exist in nearly equimolar concentrations in solution and in bulk in the solid state.

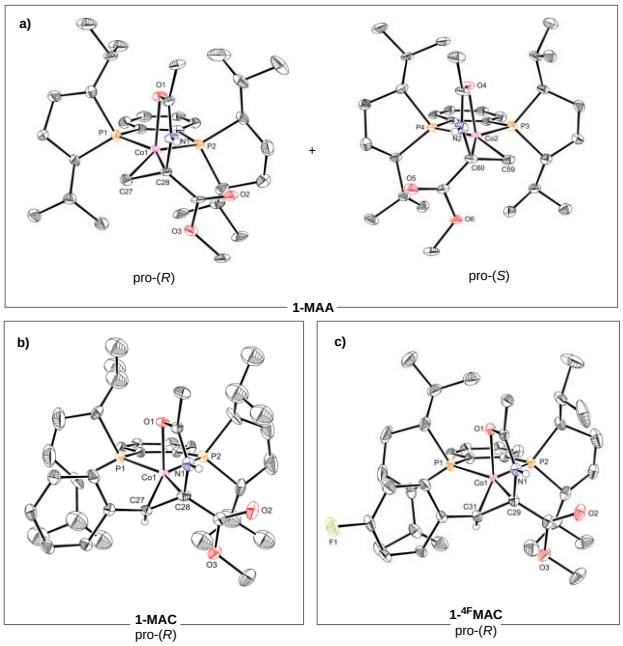

Figure 1. Solid-state structures of a) (*R*,*R*)-(^{iPr}DuPhos)Co(MAA) (**1-MAA**), b) (*R*,*R*)-(^{iPr}DuPhos)Co(MAC) (**1-MAC**), and c) (*R*,*R*)-(^{iPr}DuPhos)Co(^{4F}MAC) (**1-^{4F}MAC**) at 30% probability ellipsoids with hydrogen atoms omitted for clarity, except for amide NH and alkenyl CH in the trisubstituted enamide.

Observation of both the pro-(*R*) and pro-(*S*) diastereomers in the unit cell of **1-MAA** and exclusively the pro-(*R*) diastereomer in the unit cells of **1-MAC** and **1-^{4F}MAC**, despite the fact that the catalytic hydrogenations of all three substrates furnished the (*S*)-alkane in high enantiomeric excess, prompted further study into the relevance of these compounds to catalysis and reactivity with hydrogen. Addition of 4 atm of H_2 to a MeOH solution of **1-MAA** generated >95% conversion to MAA-H_2 (MAA-H_2 = *N*-acetylalanine methyl ester) in 80% enantiomeric excess (*ee*) (*S*), along with a new, unidentified paramagnetic cobalt compound (Scheme 3). Stoichiometric hydrogenation of **1-MAC** with 4 atm of H_2 in MeOH produced >95% conversion to MAC-H_2 (MAC-H_2 = *N*-acetylphenylalanine methyl ester) in 70% *ee* (*S*) along with the formation of a new paramagnetic cobalt product. Similarly, addition of 4 atm of H_2 to a MeOH solution of **1-^{4F}MAC** gave >95% conversion and 70% *ee* (*S*).

While these enantiomeric excesses are significantly lower than those obtained from the catalytic reactions and the exact ratio of cobalt-enamide diastereomers in solution is unknown, hydrogenation to primarily (*S*) product from a mixture of pro-(*R*) and pro-(*S*) diastereomers could indicate that cobalt-enamide diastereomers are interconverting in solution, similar to the conclusions reported for cationic rhodium catalysts.[45] One possible explanation for the lower *ee*s in the stoichiometric reaction is that diastereomer interconversion in the catalytic cycle is facilitated by exchange with free substrate in solution.[46] Accordingly, addition of 10 equivalents of MAC to a benzene-d_6/THF solution of isolated **1-^{4F}MAC** showed conversion to **1-MAC** and liberation of free ^{4F}MAC in a matter of minutes as observed by ^{1}H and ^{19}F NMR, demonstrating rapid exchange of

bound enamide with free enamide in solution. Our laboratory has previously studied the kinetics of ligand exchange between **1-COD**-d_{12} and free cyclooctadiene in solution, determining that exchange occurs through a dissociative pathway.[47]

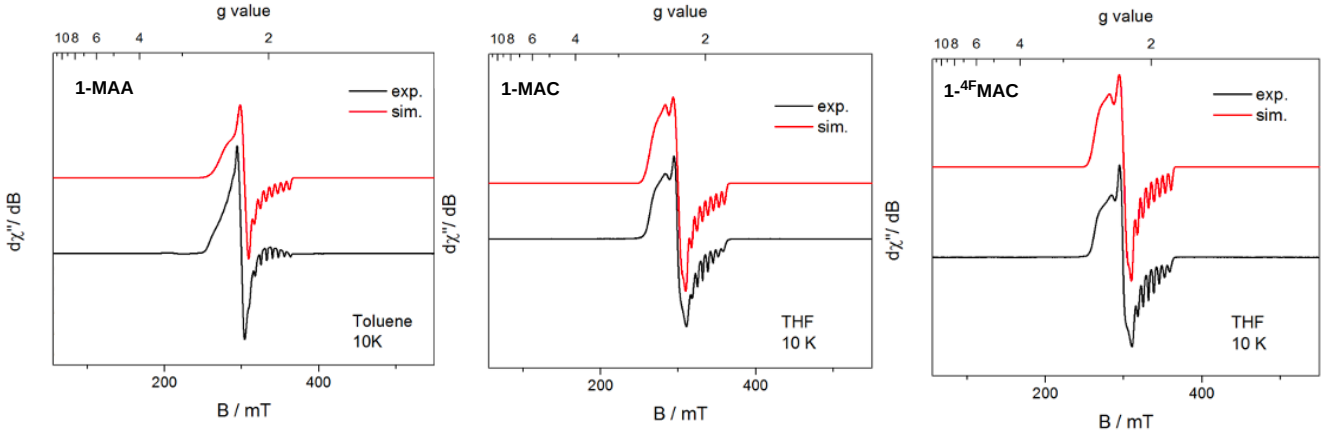

Figure 2. X-band EPR spectra of (*R*,*R*)-(^{iPr}DuPhos)Co(MAA) (**1-MAA**) (simulation parameters: g_x = 2.00, g_y = 2.23, g_z = 2.38; g_{strain} = [0.025, 0.045, 0.21]; A_{xx} = 215 MHz, A_{yy} = 0 MHz, A_{zz} = 0 MHz; A_{strain} = [30 0 0]), (*R*,*R*)-(^{iPr}DuPhos)Co(MAC) (**1-MAC**) (simulation parameters: g_x = 2.00, g_y = 2.23, g_z = 2.44; g_{strain} = [0.027, 0.078, 0.088]; A_{xx} = 198 MHz, A_{yy} = 0 MHz, A_{zz} = 103 MHz; A_{strain} = [0 0 37]), and (*R*,*R*)-(^{iPr}DuPhos)Co(^{4F}MAC) (**1-^{4F}MAC**) (simulation parameters: g_x = 2.00, g_y = 2.22, g_z = 2.45; g_{strain} = [0.025, 0.072, 0.087]; A_{xx} = 200 MHz, A_{yy} = 0 MHz, A_{zz} = 102 MHz; A_{strain} = [0 0 25]) at 10 K. Microwave frequency = 9.38 GHz, power = 0.02 mW, and modulation amplitude = 0.4 mT/100 kHz.

Additional support for the role of excess enamide in increasing the rate of diastereomer interconversion is discussed later in this manuscript in the context of H_2 pressure effects.

Scheme 3. Stoichiometric hydrogenation of (*R*,*R*)-(^{iPr}DuPhos)Co(enamide) complexes.

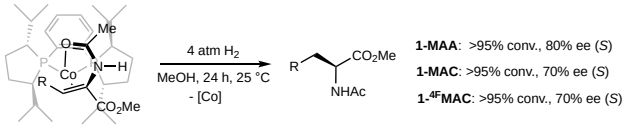

The stoichiometric experiments described above demonstrated the competency of the bis(phosphine) cobalt-enamide complexes to undergo productive reactions with H_2, albeit to yield hydrogenated products with reduced enantiomeric excesses as compared to optimized catalytic conditions, rendering their relevance to catalysis inconclusive. Subsequently, catalytic experiments were performed to evaluate the competency of **1-enamide** compounds as precatalysts. Each of the bis(phosphine) cobalt-enamide complexes was evaluated as a precatalyst for the catalytic hydrogenation of its respective enamide. Catalytic hydrogenation of each enamide was performed with either **1-COD** or its respective **1-enamide** complex as precatalyst and gave nearly identical results in terms of both yield and enantioselectivity (Scheme 4). These results demonstrate that the bis(phosphine) cobalt-enamide complexes are competent precatalysts for asymmetric hydrogenation, providing access to the active catalytic cycle as efficiently as the previously reported precatalyst, **1-COD**.[6] However, additional experiments were required to determine whether the bis(phosphine) cobalt-enamide complex serves as an active catalyst species (unsaturated pathway) or simply a precatalyst that is converted to a Co(II)-dihydride (dihydride pathway, Scheme 3) or some other catalytically active species.

Scheme 4. Catalytic hydrogenation of enamides by (*R*,*R*)-(^{iPr}DuPhos)Co(enamide).

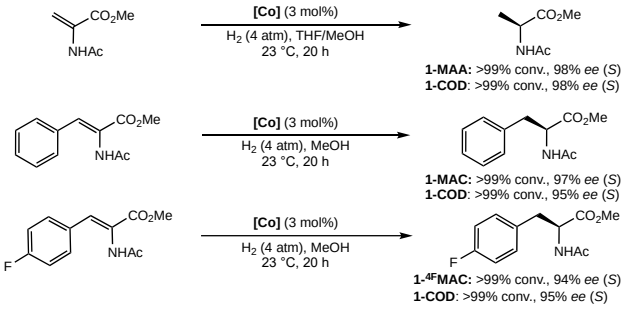

Synthesis, Characterization, and Evaluation of a Bis(phosphine) Cobalt(II)-Dihydride Bimetallic Complex. To evaluate the possibility of a dihydride pathway in cobalt-catalyzed asymmetric enamide hydrogenation, the synthesis of neutral cobalt hydride complexes was targeted as these compounds are expected to be catalytic intermediates. The initial synthetic approach focused on the hydrogenation of bis(phosphine) cobalt(II) dialkyl complexes. Addition of 4 atm of H_2 to a pentane solution of (*R*,*R*)-(^{iPr}DuPhos)Co(CH_2SiMe_3)$_2$ resulted in a rapid color change from orange to purple, furnishing a dark purple solid (Scheme 5). Cooling a saturated diethyl ether solution of the product at -35 ºC deposited single crystals suitable for X-ray diffraction. The solid-state structure (Figure 3) identified the product as the dinuclear cobalt complex with bridging hydrides, [(*R*,*R*)-(^{iPr}DuPhos)Co]$_2$(μ_2-H)$_3$(H) (**2**). The distance between the two cobalt atoms is 2.266(2) Å, consistent with a Co–Co bond.[48] While only three bridging hydrides were located on the Fourier difference map, the number of hydrides was determined with a Toepler pump experiment. A comproportionation reaction between two equivalents of (*R*,*R*)-(^{iPr}DuPhos)$CoCl_2$ and one equivalent of the hydride dimer resulted in the formation of [(*R*,*R*)-(^{iPr}DuPhos)CoCl]$_2$[6]and H_2 gas, and quantitation of the H_2 by

Toepler pump analysis established a 2:1 ratio of hydride:cobalt. The benzene-d_6 ^{1}H NMR spectrum of **2** exhbiited features expected for a diamagnetic compound, consistent with antiferromagnetic coupling between two low-spin cobalt(II) centers, suggesting that the compound persists as a dimer in solution. A related compound has been reported by Fryzuk and coworkers for [(dippp)Co]$_2$(H)(μ-H)$_3$ (dippp = di(isopropyl)phosphinopropane).[49]

Scheme 5. Synthesis of [(*R*,*R*)-(^{iPr}DuPhos)Co]$_2$(μ$_2$-H)$_3$(H).

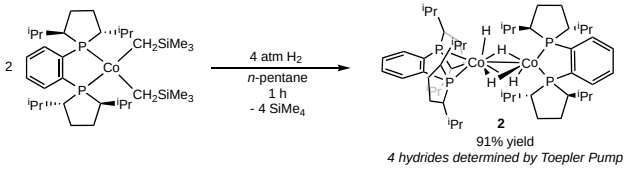

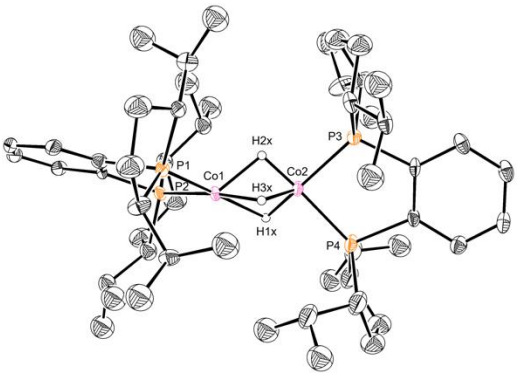

Figure 3. Solid-state structure of [(*R*,*R*)-(^{iPr}DuPhos)Co]$_2$(μ$_2$-H)$_3$(H) (**2**) at 30% probability ellipsoids with hydrogen atoms, except for the bridging cobalt-hydrides, omitted for clarity.

Isolated **2** was evaluated for its reactivity towards enamide insertion. Addition of 4 equivalents of MAA to a 1:1 THF-MeOH solution of **2** after 24 hours at room temperature resulted in a color change from deep purple to pale brown. THF was included as a cosolvent in these reactions as **2** was insoluble in MeOH. Analysis of the resulting product mixture by ^{1}H NMR spectroscopy demonstrated that 11% of the starting enamide (22% conversion as compared to cobalt) was converted to MAA-H$_2$ in 55% *ee* favoring the (*S*) alkane. Repeating this experiment in benzene-d_6 did not result in detection of H_2 gas as judged by ^{1}H NMR spectroscopy. Similarly, treatment of **2** with four equivalents of MAC under the same conditions converted 38% of the starting enamide (76% conversion as compared to cobalt) to MAC-H$_2$ in just 10% *ee*, again favoring the (*S*) alkane (Scheme 6). Treatment of **2** with four equivalents of ^{4F}MAC under the same conditions also converted 26% of the starting enamide (52% conversion as compared to cobalt) to ^{4F}MAC-H$_2$ in just 22% *ee*, again favoring the (*S*) alkane (Scheme 6). Repeating this experiment in an open vial produced similar conversion, suggesting that enamide insertion into the dihydride occurs (rather than H_2 reductive elimination, enamide coordination and reaction with stoichiometrically formed H_2. Because the ^{1}H NMR spectrum was uninformative, EPR spectroscopy was used to determine the cobalt-containing product of enamide insertion into **2**. Unsurprisingly, addition of 10 equivalents of ^{4F}MAC with **2** in a MeOH/THF (1:1) solution for one hour generated an EPR spectrum that matched that for isolated **1-^{4F}MAC**. This result demonstrates that upon reduction of Co(II) to Co(0) and alkane release, free enamide coordinates to the Co(0) center. While these reactions demonstrate some competence of **2** towards alkene insertion, the relatively low *ee*s obtained from these insertion reactions raised questions about the relevance of **2** to catalytic hydrogenation.

Scheme 6. Reactions of enamides with [(*R*,*R*)-(^{iPr}DuPhos)Co]$_2$(μ$_2$-H)$_3$(H).

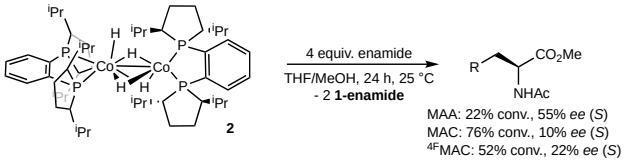

The dicobalt tetrahydride, **2** was also evaluated as a precatalyst for the asymmetric hydrogenation of each enamide. Reaction of 4 atm of H_2 with a 0.20 M solution of MAA with **2** (1.5 mol% **2**, 3 mol% cobalt) in THF/MeOH (1:1) for 20 hours resulted in 100% conversion to MAA-H$_2$ in 92% *ee* favoring the (*S*) alkane. Hydrogenation of a 0.20 M solution of MAC with 2 mol% of **2** under 4 atm of H_2 in THF-MeOH produced 96% conversion to MAC-H$_2$ with 90% *ee* favoring the (*S*) alkane. Performing the same catalytic experiment with ^{4F}MAC produced 82% conversion to ^{4F}MAC-H$_2$ with 92% *ee* favoring the (*S*) alkane. Taken together, these results demonstrate that **2** is a competent precatalyst for enamide hydrogenation. The slightly diminished enantioselectivities demonstrated in all three catalytic reactions as compared to those catalyzed by **1-COD** or any of the **1-enamide** complexes, suggest that **2** may perform a single-turnover insertion event with low selectivity before entering the active catalytic cycle.

In-Situ Reaction Monitoring to Determine the Catalyst Resting State. Stoichiometric and catalytic experiments demonstrated that both cobalt-enamide and cobalt-dihydride complexes were synthetically accessible and were competent towards their respective stoichiometric reactions (hydrogenation or enamide insertion, albeit with lower enantiomeric excesses), and were effective precatalysts. Therefore, additional experiments were required to differentiate between potential pathways. Determination of the catalyst resting state is also critical for distinguishing these pathways. Due to the paramagnetism of the cobalt(0) and (II) complexes, a combination of experiments was required to determine the catalyst resting state (Scheme 7a) as the ^{1}H NMR spectra were broad and featureless.

Due to the distinct absorbance features exhibited by the previously isolated cobalt precatalysts, reaction monitoring by UV/visible spectroscopy was performed (Scheme 7b). A gas-adapted UV/visible cuvette was used for these measurements (see SI for details).[50,51] With 3 mol% of **1-COD** as the precatalyst, the hydrogenation of 0.10 mmol of ^{4F}MAC was monitored under 1 atm of H_2 at 23 ºC. Rapid consumption of **1-COD** was observed, as was a new cobalt complex with an absorption maximum centered in the solvent region. This peak corresponded to the same spectroscopic feature measured for independently prepared **1-^{4F}MAC**, supporting the role of this compound as the catalyst resting state. Analogous experiments with **1-COD** for the hydrogenation of MAA generated an absorption maximum in the solvent region,

consistent with the spectroscopic signatures for independently prepared **1-MAA**.

To provide additional support for these experiments, freeze-quench X-band EPR experiments were conducted on active catalytic mixtures (Scheme 7c). Specifically, a J. Young-adapted EPR tube was charged with a 1:1 THF/MeOH solution of ^{4F}MAC and **1-COD** (5 mol%). Addition of 4 atm of H_2 was followed by several minutes of vigorous shaking to ensure thorough mixing of H_2 and the contents were then frozen in liquid nitrogen. The X-band EPR spectrum of the frozen glass at 10 K exhibited a distinct rhombic feature with diagnostic ^{59}Co hyperfine coupling. Simulation of the experimental spectrum established that the major feature observed was identical to the EPR spectrum of authentic **1-^{4F}MAC**, confirming the (^{iPr}DuPhos)cobalt-enamide complex as the catalyst resting state. Importantly, repeating an identical freeze-quench EPR experiment with catalyst initiation from **2**, rather than **1-COD**, similarly demonstrated **1-^{4F}MAC** as the catalyst resting state. This result corroborates the conclusions of the previous section, that while **2** may be able to enter the active catalytic cycle through subsequent formation of **1-enamide**, **2** is not an on-cycle intermediate. Performing an identical experiment with MAC and **1-COD** demonstrated that **1-MAC** was the major feature also supporting the cobalt enamide compound as the catalyst resting state.

Scheme 7. Catalyst resting state analysis using UV/visible and EPR spectroscopies.

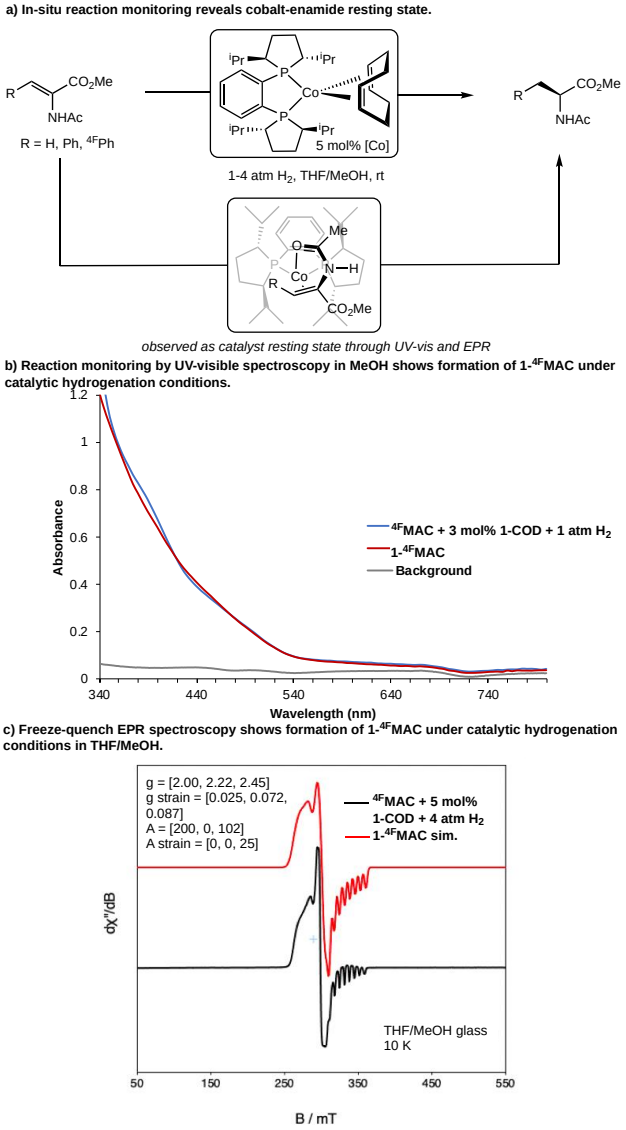

Taken together, these experiments establish bis(phosphine) cobalt-enamide complexes as the catalyst resting states in the catalytic hydrogenation reactions with all three enamides used in this study. Cobalt-enamide complexes are expected to be intermediates along the unsaturated pathway (where cobalt-enamide complexation occurs before hydrogen activation), but not along a dihydride pathway. Therefore, the observation of cobalt-enamide complex as the catalyst resting state suggests that a dihydride pathway may not be relevant in the catalytic hydrogenation reaction.

Rate Law for the Bis(Phosphine) Cobalt-Catalyzed Asymmetric Hydrogenation of Enamides. To gain additional insight into the mechanism of cobalt-catalyzed asymmetric hydrogenation, the experimental rate law for the hydrogenation of ^{4F}MAC was determined. Initial experiments were performed at relatively low (1-4 atm) H_2 pressures in J-Young NMR tubes with constant gas mixing to avoid complications from mass transfer.[52] ^{4F}MAC was selected as the representative enamide, given its lower reactivity to facilitate reaction monitoring, and conversions were determined in proteo-MeOH by relative integrations of ^{4F}MAC and ^{4F}MAC-H_2 by ^{19}F NMR spectroscopy. **1-^{4F}MAC**

was used as the precatalyst, modeling the rhodium(I) kinetic analysis described by Landis and Halpern,[26] in an attempt to minimize complications from precatalyst activation. Variable time normalization analysis (VTNA) of reaction time courses as described by Burés were applied[53] in which the initial concentrations of ^{4F}MAC, H_2, and **1-^{4F}MAC** were systematically varied. Analysis of the resulting overlay plots established the rate law show in in eq 1 (Figure 4).

rate = k[**1-^{4F}MAC**]^1[^{4F}MAC]^0[H_2]^1 (1)

To verify that this rate law is maintained at higher pressures of H_2 that are used under more optimized conditions, reaction progress experiments were performed in a high-pressure reactor. Due to the higher gas pressure, precatalyst loadings were lowered and varied between 0.5 and 2 mol%, ^{4F}MAC concentrations were varied between $2.1x10^{-4}$ and $8.4x10^{-4}$ M, and the H_2 pressure was maintained at 500 psi. Each measurement was made in triplicate. Data points were obtained after quenching the hydrogenation after 5 minutes and filtration through alumina and quantification of conversion by ^{19}F and ^{1}H NMR spectroscopies. The data also supported the rate law presented in equation 1 with a positive dependence on catalyst loading and no dependence on substrate concentration. Identical reactions at 100 and 200 psi demonstrated a positive dependence on the concentration of H_2, again in agreement with equation 1.

The rate law presented in eq 1 is consistent with a rate-determining step involving activation of H_2 by the cobalt catalyst. The pseudo-zero order dependence on enamide concentration (rather than an inverse order), in combination with the observed cobalt-enamide resting state, suggests enamide saturation kinetics rather than a mechanism where complete enamide dissociation is required prior to activation of H_2. These results are therefore inconsistent with a dihydride pathway, in which cobalt reacts with H_2 prior to enamide binding. On the other hand, these results could support an unsaturated pathway, in which formation of a cobalt-enamide complex occurs prior to rate-limiting H_2 activation. These kinetic results are consistent with those reported by Landis and Halpern in their studies of rhodium(I)-catalyzed asymmetric alkene hydrogenation.[26]

H_2 Pressure Effects. A key observation by Landis and Halpern in their work on the rhodium-catalyzed unsaturated hydrogenation pathway was an inverse dependence of pressure on product enantioselectivity arising from competition between diastereomer interconversion and H_2 activation. Accordingly, H_2 pressure dependence studies were performed on both the stoichiometric hydrogenation of **1-enamide** and the catalytic hydrogenation of enamides by **1-COD**.

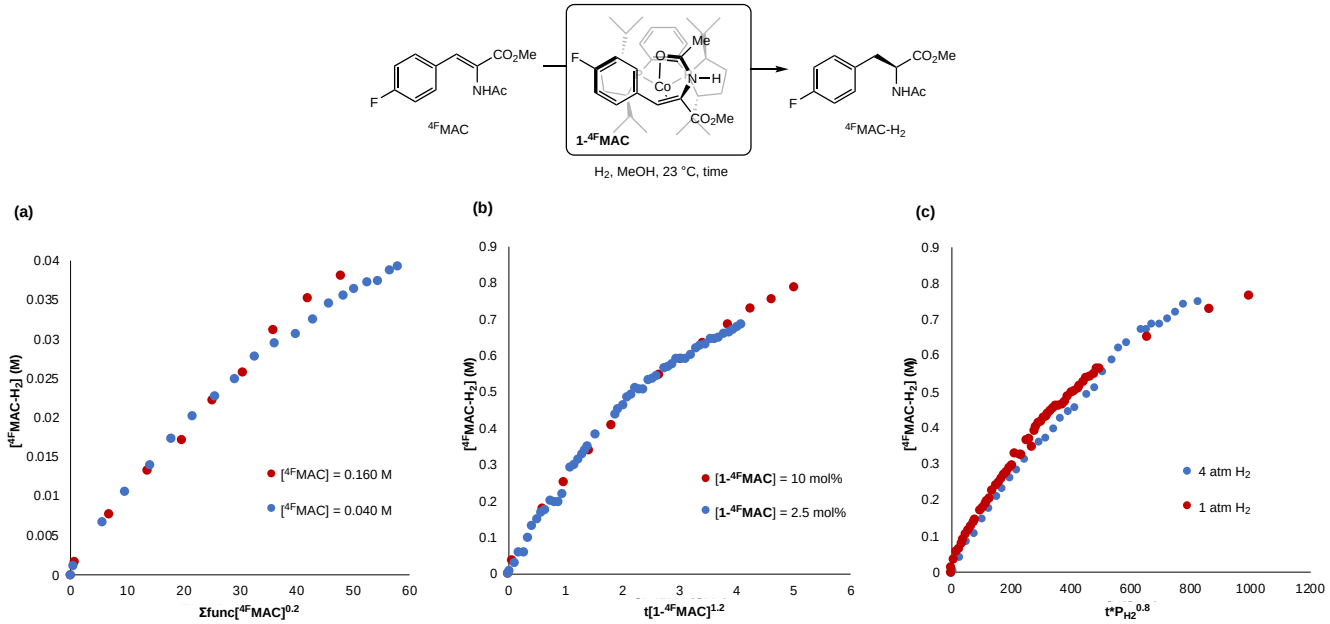

Figure 4. Overlay plots obtained from VTNA for the determination of the rate law for the hydrogenation of ^{4F}MAC with H_2 with **1-^{4F}MAC** as the precatalyst: (a) order in ^{4F}MAC, (b) order in **1-^{4F}MAC**, (c) order in H_2 pressure.

The hydrogenation of identical samples of isolated **1-^{4F}MAC** in MeOH was performed at 100, 200, and 400 psi in a high-pressure reactor, and gave enantioselectivities of 83%, 80%, and 75% *ee* (*S*), respectively (Table 2). The observation of higher enantioselectivites at lower pressures is consistent with competitive rates of diastereomer interconversion and H_2 activation. In contrast, catalytic experiments involving the hydrogenation of enamide by **1-COD** (3 mol%) in MeOH showed little to no dependence of the enantioselectivity on the H_2 pressure. Hydrogenation of MAA at 100, 200, 300, and 400 psi gave corresponding enantioselectivities of 95%, 95%, 94%, and 90% *ee* (*S*). Hydrogenation of MAC and ^{4F}MAC gave consistent enantioselectivities of 96% and 95% *ee* (*S*), respectively, across a pressure range of 100-400 psi. These results suggest that under standard catalytic conditions with a large excess of substrate, the rate of diastereomer interconversion is significantly faster than the rate of H_2 activation, such that the observed enantioselectivity exhibits little dependence on H_2 pressure. Based on this model, performing the hydrogenation reaction at low substrate concentration and high H_2 pressure should produce a lower enantioselectivity as compared to the standard catalytic reaction. Accordingly, hydrogenation of ^{4F}MAC by **1-COD** (20 mol%) at 400 psi of H_2 resulted in diminished

enantioselectivity of 86% *ee* (*S*), as compared to the standard catalytic reaction.

Table 2. H_2 pressure effects on enantioselectivities.

Experiment	H_2 Pressure (psi)	Enantiomeric Excess (*ee* (*S*))
1-^{4F}MAC (stoichiometric)	100	83%
	200	80%
	400	75%
MAA by **1-COD** (3 mol%)	100	95%
	200	95%
	300	94%
	400	90%
MAC by **1-COD** (3 mol%)	100	96%
	200	96%
	400	96%
^{4F}MAC by **1-COD** (3 mol%)	100	95%
	200	95%
	300	95%
	400	95%
^{4F}MAC by **1-COD** (20 mol%)	400	86%

Taken together, these results demonstrate that free enamide substrate likely plays a role in diastereomer interconversion. In the absence of a large excess of substrate, diastereomer interconversion is slowed and its rate becomes competitive with H_2 activation, resulting in overall lower enantioselectivities. Under standard catalytic conditions, the ratio of free substrate to cobalt is high and the rate of diastereomer interconversion is much faster than H_2 activation which in turn leads to high enantioselectivities. In an intermediate range where the cobalt:substrate ratio is lower and the H_2 pressure remains high, an intermediate enantioselectivity is obtained. These results explain why stoichiometric hydrogenation of isolated **1-enamide** complexes produce lower enantiomeric excesses than the catalytic reactions.

Deuterium Labeling Studies. With the catalyst resting state and reaction rate laws established, deuterium-labeling studies were conducted to gain additional insight into the reaction between hydrogen gas and cobalt complexes. Catalytic reduction of all three enamides with **1-COD** and D_2 in MeOH produced 1:1 deuterium incorporation into both the α- and β-positions of the corresponding alkane, demonstrating that reducing equivalents for the alkene are provided entirely from the gas without solvent proton donation (Scheme 8a).

Measurement of the deuterium kinetic isotope effect (KIE) was performed using an identical experimental set-up to that used for the NMR kinetics with **1-^{4F}MAC** as the precatalyst and ^{4F}MAC as representative substrate in MeOH. To separate solutions of ^{4F}MAC (0.080 M) and **1-^{4F}MAC** (0.0040 M, 5 mol%) in MeOH (0.5 mL) in J. Young NMR tubes was added 4 atm H_2 or D_2 with each reaction performed in triplicate. Reaction progress was monitored by ^{19}F NMR by relative integrations of starting material and product. Initial rate experiments demonstrated an H_2/D_2 KIE of 1.2(2) at 23 ºC (Scheme 8b). This value is similar to the k_H/k_D of 1.22 reported by Parker and Brown[42] for the hydrogenation of *Z*-(α)-acetamidocinnamic acid with $[Rh(DIPHOS)]^+$ (DIPHOS = 1,2-Bis(diphenylphosphino)ethane) catalyst and the value of 1.04 reported by Landis and Brauch[54] for the hydrogenation of MAA with $[Rh(DIPHOS)(NBD)][BF_4]$ (NBD = norbornadiene).

Scheme 8. Deuterium labeling studies.

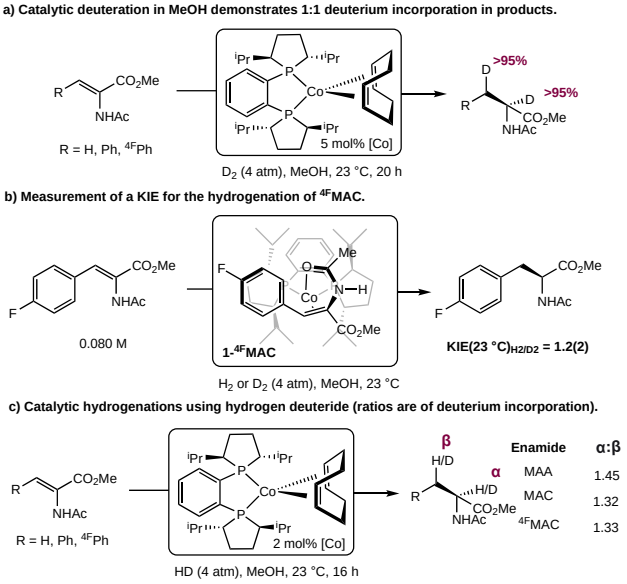

Catalytic hydrogenations were also performed with hydrogen deuteride (HD) to probe directional specificity in the enamide hydrogenation. All three substrates were hydrogenated using **1-COD** as the precatalyst in MeOH. ^{1}H and ^{2}H NMR spectroscopies were used to determine relative proton and deuterium incorporations in the α- and β-positions. Quantitative ^{13}C NMR spectroscopy and high-resolution mass spectrometry were used to determine the relative quantities of H_2, HD, DH, and D_2 products (see SI for details). For MAA, addition of 4 atm of HD to a solution of MAA (0.10 M) and 2 mol% of **1-COD** at room temperature for 16 hours resulted in preferential deuterium incorporation into the α- over the β-position in a 1.45:1 ratio (Scheme 8c). To rule out the possibility that the preferential incorporation was the result of reversible alkyl hydride formation in methanol, the reaction was repeated in THF and similar 1.28:1 ratio for deuterium incorporation into the α- over β-positions was observed, respectively. Identical experiments with MAC and ^{4F}MAC with **1-COD** in MeOH showed similar preference for the α-position (1.32:1 and 1.33:1 respectively). For comparison, the catalytic hydrogenation of MAA and MAC by $[Rh(DIPHOS)(NBD)][BF_4]$ was reported to give a 1.21:1 and 1.33:1 preference, respectively, for the α-position in THF.[49] These results support an irreversible H_2 addition step to the cobalt-enamide complex.[49]

Mechanistic Interpretation of Experimental Results. Taken together, the experimental results provide insights into the mechanism of cobalt-catalyzed asymmetric hydrogenation. Stoichiometric and catalytic reactions with both cobalt-enamide (**1-enamide**) and cobalt-dihydride (**2**) complexes demonstrated their catalytic competency and as such provide little distinction about whether a dihydride or an unsaturated pathway is operative. The observation of a cobalt-enamide resting state during catalytic hydrogenation suggests that enamide coordination to the cobalt occurs prior to H_2 activation, favoring an unsaturated over a dihydride pathway. Reaction kinetic analyses support saturation in enamide, and a rate-determining step involving H_2 activation by a cobalt-enamide complex. Again, this supports an unsaturated pathway, whereby formation of the cobalt-enamide complex formation precedes H_2 activation. Hydrogen pressure effect studies on product

enantioselectivity under stoichiometric, catalytic, and intermediate conditions where the substrate to catalyst ratio is changed, established that in the presence of large excesses of substrate, interconversion of cobalt-enamide diastereomers occurs at a rate that is much faster than H_2 activation. Therefore, product enantioselectivity is a reflection not of the relative abundance of cobalt-enamide diastereomers in solution, but rather of their relative rates of reaction with H_2, consistent with the anti-"lock-and-key" concept.

These observations are also consistent with the observation of the "wrong" pro-(*R*) diastereomer in the unit cells of all three **1-enamide** solid-state structures, although paramagnetism precludes determination of solution-state diastereomeric ratios. Deuterium labeling experiments demonstrate that the protons transferred to the product are derived from hydrogen gas, with a KIE similar to those observed previously in rhodium unsaturated pathways. Likewise, HD partitioning ratios are indicative of a 2,1-insertion step. Taken together, each of these results is consistent with an unsaturated pathway, while many results are inconsistent with a dihydride pathway.

It is important to note that other pathways, aside from the idealized limits of dihydride and unsaturated pathways are also possible. In contrast to the rapid equilibration of cobalt-enamide diastereomers prior to H_2 activation, it is possible that interchange between the pro-(*R*) and pro-(*S*) pathways occurs following activation of H_2, such as has been proposed by Gridnev and Imamoto.[35] In this case, enantio-interconversion occurs after H_2 activation but before migratory insertion through reversible partial dissociation and reassociation of the enamide to the metal through the C=C bond. However, this mechanism is inconsistent with the observed dependence of cobalt-enamide hydrogenation enantioselectivity on hydrogen pressure. It is also possible that partial enamide dissociation takes place earlier in the catalytic cycle, such as in the H_2 activation step. This possibility cannot be ruled out based on the available experimental data. While D_2 experiments exclude the possibility of heterolytic hydrogen activation, it is unclear what role, if any, the methanol solvent may play in diastereomer interconversion, enamide chelation dynamics, or stabilization of intermediates. Other pathways initiated from cobalt-enamide complexes may also be possible, such as an all cobalt(II) metallacycle mechanism involving activation of the N–H bond, or a pathway involving tautomerization of the enamide to its imine form. Neither of these pathways is readily excluded by experiment. Furthermore, the nature of the H_2 activation step is difficult to evaluate based on experiments alone. Products of formal oxidative addition of H_2, such as the dihydride alkene or monohydride alkyl intermediates observed in diamagnetic rhodium catalysis, have not been observed with the paramagnetic cobalt catalysts. The origin of enantioselection is also challenging to establish based on experiment alone. While the H_2 pressure effect studies (in combination with the catalyst resting state and rate law) suggest that enantioselection arises from the H_2 activation step, the exact interactions that lead to the differentiation between the pro-(*R*) and pro-(*S*) pathways remain unclear. Therefore, density functional theory calculations were conducted to provide insights into the open questions about enamide chelation dynamics, role of protic solvent, cobalt oxidation-state changes, H_2 activation modes, and enantioselectivity.

Density Functional Theory Calculated Mechanistic Pathway. To learn more nuanced information about the steps of the catalytic cycle, density functional theory calculations (PBE0-D3BJ,IEFPCM[methanol]) were performed on the [(*R*,*R*)-(^{iPr}DuPhos)Co]-catalyzed asymmetric hydrogenation reaction with MAA as a representative substrate. Several possible mechanistic pathways were evaluated using DFT methods on the full molecular systems. Detailed schematic drawings and energies for all pathways are found in the Supporting Information (SI, Scheme S92-99). A dihydride pathway could be ruled out through calculation, as the proposed (*R*,*R*)-(^{iPr}DuPhos)CoH_2 intermediate is 24.0 kcal/mol higher in energy than 1-MAA (unbolded to signify theoretical, Figure S94), in agreement with experimental findings. Thus, hydrogenation pathways begin from 1-MAA.

The computed structure of 1-MAA has the enamide coordinated to the cobalt by the C=C double bond and the oxygen of the amido group, as observed in the X-ray structure of **1-MAA** (Figure 1). Interestingly, there is only a 0.2 kcal/mol energy difference between the pro-(*R*) and pro-(*S*) diastereomers of 1-MAA, suggesting that they will be formed in approximately equal quantities (Figure S96), which may explain the crystallographically observed diastereomeric mixture of 1:1 (Figure 1a). Calculations establish a high dissociation energy of 56.6 kcal/mol for the MAA substrate (Figure S95), indicating a strong Co-enamide interaction. Attempts to calculate structures with partial dissociation of the enamide in the presence of ligating methanol were unsuccessful, however, enamide coordination solely through the carbonyl groups leads to a state 23.8 kcal/mol higher in energy than 1-MAA, indicating that such structures are not relevant during the catalytic cycle.

With 1-MAA as the starting point, three mechanistic pathways were considered: a classical redox Co(0/II) mechanism **A**, a Co(0/II) imine mechanism **B**,[55] and a non-redox metallacycle pathway **C** where cobalt exhibits the +2 oxidation state during the whole catalytic cycle.[56] The DFT calculations were performed with an explicit MeOH molecule added to the model, as we have shown for related calculations on (*R*,*R*)-(^{Ph}BPE)Co(MAA) that inclusion of a polar solvent molecule stabilizes the charges at the rate-limiting transition states and thus affects the final energies and enantioselectivities.[57,58]

The first considered pathway is the redox-type mechanism **A** (Scheme 9). In the initial step of mechanism **A**, coordination of H_2 to **1-MAA** occurs through TS-H_2 to form a 1-MAA-dihydrogen (σ-bound H_2) intermediate. Importantly, H_2 does not undergo oxidative addition to form a Co(II)-dihydride, as formation of the σ-complex is preferred by 21.5 kcal/mol over the dihydride (Figure S97). Subsequently, oxidative hydride transfer to the *β*-carbon occurs to give a 1-alkyl-hydride intermediate (Figure 5). This step is found to be rate-

Scheme 9. Calculated Co(0)/(II) redox cycling pathway for the hydrogenation of MAA (mechanism A) (barriers relative to 1-MAA, 298K, PBE0-D3BJ/IEFPCM(methanol)).

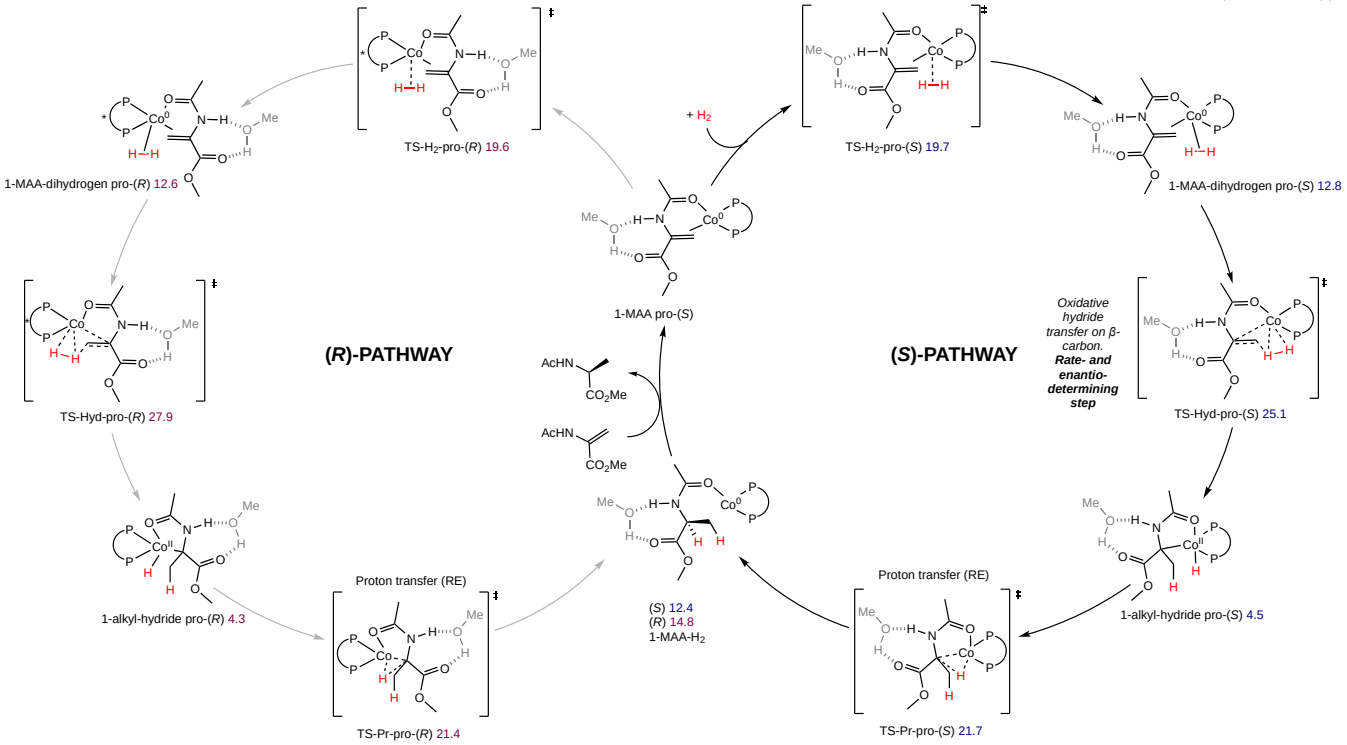

limiting for mechanism **A** with an overall barrier of 25.1 kcal/mol for the formation of the (*S*)-product and 27.9 kcal/mol for the formation of the (*R*)-product. In the last step, reductive elimination releases the product and regenerates the 1-MAA species. An overall barrier of 25.1 kcal/mol for the (*S*)-pathway would be feasible at the experimental temperature of 298 K (based on the discussion by Baik and coworkers, a reasonable conversion at 298 K requires a barrier around 25 kcal/mol or lower).[59] Analysis of the optimized geometries shows that the preference for the (*S*)-TS-Hyd transition state can be ascribed to stronger interactions between cobalt and a carbonyl of the enamide, as well as more favorable C–H…O interactions, together with less steric clash with the ^{i}Pr substituents on the DuPhos ligand compared to (*R*)-TS-Hyd (Figure 5, bottom). The computed *ee* of 98.2% for MAA is in excellent agreement with the experimental *ee* of 98.5% (*S*).

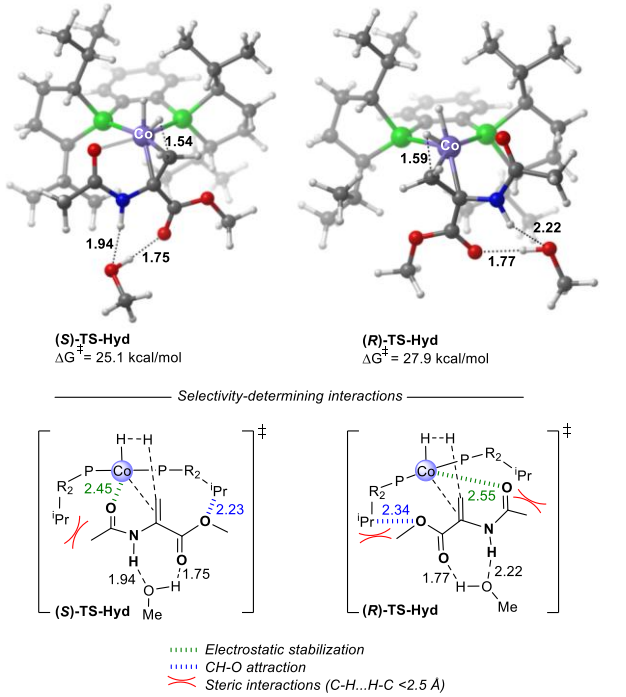

Figure 5. Optimized pro-(*S*) and pro-(*R*) transition states for oxidative hydride transfer for (*R*,*R*)-(^{iPr}DuPhos)Co-catalyzed hydrogenation of MAA by redox mechanism **A**, with a hydrogen-bonded MeOH (barriers relative to 1-MAA, 298K, PBE0-D3BJ,IEFPCM[methanol]).

The computed energies and selectivities support redox-type mechanism **A**, which also agrees well with other experimental results (*vide supra*), including a diastereomeric cobalt-enamide resting state and a first-order dependence on the H_2 concentration. In addition, the results of the HD

hydrogenation experiments are quantitatively reproduced by Mechanism **A**. Based on the difference in zero-point energies, cobalt should have a larger difference in bond strength and a larger KIE for Co–D versus Co–H, as compared to C–D versus C–H. Therefore, the predicted oxidative hydride transfer to the β-position of 1-MAA-dihydrogen in the rate-determining TS-Hyd should result in preferential transfer of H to the β-carbon and D to the cobalt, ultimately resulting in higher incorporation of deuterium in the α-position of the product. Calculations on TS-Hyd with replacement of one hydrogen by deuterium support a 1.17:1 preference for initial H transfer versus initial D transfer from HD to the Cβ of MAA, in agreement with the experimental results. Preferential olefin insertion into the M–H versus M–D bond in the initial step during HD hydrogenation is well-precedented in rhodium catalysis.[28,29,42,49] With cobalt, the preferential deuterium incorporation in the α-position also supports formation of 1-alkyl-hydride following oxidative hydride transfer.

Two other mechanistic pathways beginning from 1-MAA were also computed but are ruled out (see SI for details). Both redox imine mechanism **B** (Figure S98) and non-redox metallacycle mechanism **C** (Figure S99) have overall computed barriers above 30 kcal/mol, inconsistent with the room temperature reaction conditions used experimentally. Additionally, both pathways would predict the wrong, (*R*) hand of the product as compared to the (*S*)-product obtained from the experimental catalytic reaction and redox mechanism **A**. These results are consistently reproduced by three different DFT protocols (SI, Table S7). Analaysis of the alternative substrate ^{4F}MAC also supported feasible barriers for mechanism **A** (Table S8), alongside a computed H_2/D_2 KIE of 1.33 (Table S9), which is in good agreement with the experimentally observed value of 1.2(2) (Scheme 8). We note that the computational results for (*R*,*R*)-(^{iPr}DuPhos)Co differ from the related (*R*,*R*)-(^{Ph}BPE)Co complex, where mechanism **C** appears to be energetically accessible for hydrogenation of MAA.[57]

To summarize, computational results support that (*R*,*R*)-(^{iPr}DuPhos)Co-catalyzed hydrogenation of MAA proceeds by an unsaturated Co(0)–Co(II) redox pathway (Scheme 9), which does not involve formation of a distinct Co-dihydride species. These conclusions are consistent with experimental results, particularly that 1-MAA is the lowest energy species along the catalytic cycle and that H_2 addition to the substrate is rate-determining. Agreement is also found with the experimental enantiomeric excess and the results of experimental hydrogenation of MAA with HD.

CONCLUSIONS

Experimental and computational mechanistic investigations on the neutral [(*R*,*R*)-(^{iPr}DuPhos)Co]-catalyzed hydrogenation of prochiral enamides have been performed. Independent syntheses established that both bis(phosphine) cobalt-enamide and -hydride complexes are stable, isolable species, which could be used productively in both catalytic and stoichiometric reactions (with diminished enantiomeric excesses in the stoichiometric reactions). Catalyst resting state analysis using UV-visible and EPR spectroscopies revealed a cobalt-enamide resting state for all three representative enamides, supporting an unsaturated pathway for enamide hydrogenation, whereby reaction with enamide precedes H_2 activation. Catalytic reaction kinetics in MeOH using VTNA techniques established a first order dependence on H_2 and bis(phosphine) cobalt-enamide concentrations, with a zero-order dependence on enamide substrate concentration. These results are consistent with reaction of H_2 with a bis(phosphine) cobalt-enamide complex as the rate-determining step, similarly in agreement with an unsaturated pathway. Deuterium-labeling experiments demonstrated a homolytic pathway for H_2 cleavage and H_2 versus D_2 kinetic isotope effects and HD partitioning experiments are consistent with irreversible and regioselective hydride transfer to the cobalt-enamide complex. Computations using MAA as representative substrate support an unsaturated pathway with **1-MAA** as the lowest energy intermediate and a rate-determining oxidative hydride transfer from a σ-bonded 1-MAA-dihydrogen complex to the β-position of the substrate, a key difference from the rhodium unsaturated pathway involving oxidative addition of H_2. Both the computational results and deuterium labeling experiments demonstrate that cobalt redox-cycling is reasonable for enamide hydrogenation with [(*R*,*R*)-(^{iPr}DuPhos)Co]-complexes. Overall, an unsaturated pathway by Co(0/II) redox cycling has been elucidated for the cobalt-catalyzed asymmetric hydrogenation of enamides. Although the term "unsaturated" as a general mechanistic descriptor is used to signal substrate coordination prior to H_2 activation, several distinctions are noted between the Co(0/II) and Rh(I/III) unsaturated mechanisms, including the charge, oxidation state and geometries of intermediates, mode of H_2 activation, and the interactions responsible for enantioselection. Nonetheless, many fundamental properties in reactivity and selectivity are consistent between the reaction mechanisms, establishing shared guiding principles for catalytic reaction design.

ASSOCIATED CONTENT

Supporting Information

The Supporting Information is available free of charge on the ACS Publications website.

Additional experimental and computational details; characterization data including NMR and EPR spectra of new compounds (PDF)

Computationally optimized geometries which can be visualized with Mercury (XYZ).

Crystallographic information for (*R*,*R*)-(^{iPr}DuPhos)Co(MAA) (**1-MAA**, 2152606), (*R*,*R*)-(^{iPr}DuPhos)Co(MAC) (**1-MAC**, 2152607), (*R*,*R*)-(^{iPr}DuPhos)Co(^{4F}MAC) (**1-^{4F}MAC**, 2152608), and [(*R*,*R*)-(^{iPr}DuPhos)Co]$_2$(μ_2-H)$_3$(H) (**2**, 2069834).

AUTHOR INFORMATION

Corresponding Authors

* **Paul J. Chirik** – *Department of Chemistry, Princeton University, Princeton, New Jersey 08544, United States; orcid.org/0000-0001-8473-2898;* Email: pchirik@princeton.edu

*** Kathrin H. Hopmann** – *Department of Chemistry, UiT – The Arctic University of Norway, N-9037 Tromsø, Norway; orcid.org/0000-0003-2798-716X;* Email: kathrin.hopmann@uit.no

Authors

Lauren N. Mendelsohn – *Department of Chemistry, Princeton University, Princeton, New Jersey 08544, United States; orcid.org/0000-0002-0596-6838;* Email: lm30@princeton.edu
Ljiljana Pavlovic – *Department of Chemistry, UiT – The Arctic University of Norway, N-9037 Trømso, Norway; orcid.org/0000-0002-0906-6298;* Email: ljiljana.pavlovic@uit.no
Hongyu Zhong – *Department of Chemistry, Princeton University, Princeton, New Jersey 08544, United States; orcid.org/0000-0002-6892-482X;* Email: hongyu.zhong@ord.chem.ethz.ch
Max R. Friedfeld – *Department of Chemistry, Princeton University, Princeton, New Jersey 08544,; orcid.org/0000-0001-5693-3705;* Email: maxfriedfeld@gmail.com
Michael Shevlin – *Department of Process Research & Development, Merck & Company, Limited, Rahway, New Jersey, 07065, United States; orcid.org/0000-0003-2566-5095;* Email: michael_shevlin@merck.com

Notes
Any additional relevant notes should be placed here.

ACKNOWLEDGMENT

Financial support was provided by the U.S. National Science Foundation Grant Opportunities for Academic Liaison with Industry (GOALI) grant (CHE-1855719). We would like to thank Dr. Matthew Winston for his helpful comments on this manuscript. This work has been supported by the Research Council of Norway (No. 300769), by the Tromsø Research Foundation (No. TFS2016KHH), by Sigma2 (No. nn9330k), and by NordForsk (No. 85378).

REFERENCES

[1] (a) Knowles, W. S. Asymmetric Hydrogenations (Nobel lecture). *Angew. Chem., Int. Ed.* **2002**, *41*, 1998–2007. (b) Noyori, R. Asymmetric catalysis: Science and Opportunities (Nobel lecture). *Angew. Chem. Int. Ed.* **2002**, *41*, 2008–2022. (c) Püntener, K.; Scalone, M. Enantioselective Hydrogenation: Applications in Process R&D of Pharmaceuticals. In: *Asymmetric Catalysis on Industrial Scale: Challenges, Approaches and Solutions*, 2nd ed.; Blaser, H.-U., Federsel, H.-J., Eds.; Wiley-VCH: Weinheim, Germany, 2010; pp 13-25.
[2] Schultz, C. S.; Krska, S. W. Unlocking the Potential of Asymmetric Hydrogenation at Merck. *Acc. Chem. Res.* **2007**, *40*, 1320–1326.
[3] Busacca, C. A.; Fandrick, D. R.; Song, J. J.; Senanayake, C. H. The Growing Impact of Catalysis in the Pharmaceutical Industry. *Adv. Synth. Catal.* **2011**, *353*, 1825–1864.
[4] Saudan, L. A. Hydrogenation Process in the Synthesis of Perfumery Ingredients. *Acc. Chem. Res.* **2007**, *40*, 1309–1319.
[5] Friedfeld, M. R.; Shevlin, M.; Hoyt, J. M.; Krska, S. W.; Tudge, M. T.; Chirik, P. J. Cobalt Precursors for High-Throughput Discovery of Base Metal Asymmetric Alkene Hydrogenation Catalysts. *Science* **2013**, *342*(6162), 1076–1080.
[6] Friedfeld, M. R.; Zhong, H.; Ruck, R. T.; Shevlin, M.; Chirik, P. J. Cobalt-Catalyzed Asymmetric Hydrogenation of Enamides Enabled by Single-Electron Reduction. *Science* **2018**, *360*, 888–893.
[7] Zhong, H.; Friedfeld, M. R.; Chirik, P. J. Synthesis and Catalytic Hydrogenation Performance of Cationic Bis(phosphine) Cobalt(I) Diene and Arene Compounds. *Angew. Chem., Int. Ed.* **2019**, *58*, 9194–9198.
[8] Zhong, H.; Shevlin, M.; Chirik, P. J. Cobalt-Catalyzed Asymmetric Hydrogenation of *α,β*-Unsaturated Carboxylic Acids by Homolytic H_2 Cleavage. *J. Am. Chem. Soc.* **2020**, *142*, 5272–5281.
[9] Du, X.; Xiao, Y.; Huang, J.-M.; Zhang, Y.; Duan, Y.-N.; Wang, H.; Shi, C.; Chen, G.-Q.; Zhang, X. Cobalt-Catalyzed Highly Enantioselective Hydrogenation of *α,β*-Unsaturated Carboxylic Acids. *Nat. Commun* **2020**, *11*, 3239–3249.
[10] Du, X.; Xiao, Y.; Yang, Y.; Duan, Y.-N.; Li, F.; Hu, Q.; Chung, L. W.; Chen, G.-Q.; Zhang, X. Enantioselective Hydrogenation of Tetrasubstituted *α,β*-Unsaturated Carboxylic Acids Enabled by Cobalt(II) Catalysis: Scope and Mechanistic Insights. *Angew. Chem. Int. Ed.* **2021**, *60*, 11384–11390.
[11] Hu, Y.; Zhang, Z.; Zhang, J.; Liu, Y.; Gridnev, I. D.; Zhang, W. Cobalt-Catalyzed Asymmetric Hydrogenation of C=N Bonds Enabled by Assisted Coordination and Nonbonding Interactions. *Angew. Chem. Int. Ed.* **2019**, *58*, 15767–15771.
[12] Hu, Y.; Zhang, Z.; Liu, Y.; Zhang, W. Cobalt-Catalyzed Chemo- and Enantioselective Hydrogenation of Conjugated Enynes. *Angew. Chem. Int. Ed.* **2021**, *60*(31), 16989–16993.
[13] (a) Vogt, D. Cobalt-Catalyzed Asymmetric Hydrovinylation. *Angew. Chem. Int. Ed.* **2010**, *49*, 7166–7168. (b) Bohn, M. A.; Schmidt, A.; Hild, G.; Dindaroglu, M.; Schmalz, H.-G. Cobalt-Catalyzed 1,4-Hydrobutadienylation of 1-Aryl-1,3-dienes with 2,3-Dimethyl-1,3-butadiene. *Angew. Chem. Int. Ed.* **2011**, *50*(41), 9689–9693. (c) Hilt, G.; Danz, M.; Treutwein, J. Cobalt-Catalyzed 1,4-Hydrovinylation of Styrenes and 1-Aryl-1,3-butadienes. *Org. Lett.* **2009**, *11*(15), 3322–3325. (d) Hilt, G.; Mesnil, F.-X.; Luërs, S. An Efficient Cobalt(I) Catalyst System for the Selective 1,4-Hydrovinylation of 1,3-Dienes. *Angew. Chem. Int. Ed.* **2001**, *40*(2), 387–389. (e) Arndt, M.; Dindaroglu, M.; Schmalz, H.-G.; Hilt, G. Gaining Absolute Control of the Regiochemistry in the Cobalt-Catalyzed 1,4-Hydrovinylation Reaction. *Org. Lett.* **2011**, *13*(23), 6236–6239. (f) Timsina, Y. N.; Sharma, R. K.; RajanBabu, T. V. Cobalt-Catalyzed Asymmetric Hydrovinylation of 1,3-Dienes. *Chem. Sci.* **2015**, *6*, 3993–4008.
[14] Duvvuri, K.; Dewese, K. R.; Parsutkar, M. M.; Jing, S. M.; Mehta, M. M.; Gallucci, J. C.; RajanBabu, T. V. Cationic Co(I)-Intermediates for Hydrofunctionalization Reactions: Regio- and Enantioselective Cobalt-Catalyzed 1,2-Hydroboration of 1,3-Dienes. *J. Am. Chem. Soc.* **2019**, *141*(18), 7365–7375.
[15] (a) Treutwein, J.; Hilt, G. Cobalt-Catalyzed [2+2] Cycloaddition. *Angew. Chem., Int. Ed.* **2008**, *47*(36), 6811–6813. (b) Nishimura, A.; Tamai, E.; Ohashi, M.; Ogoshi, S. Synthesis of Cyclobutenes and Allenes by Cobalt-Catalyzed Cross-Dimerization of Simple Alkenes with 1,3-Enynes. *Chem. Eur. J.* **2014**, *20*(22), 6613–6617. (c) Röse, P.; Hilt, G. Cobalt-Catalyzed Bond Formation Reactions; Part 2. *Synthesis* **2016**, *48*(04), 463–492.
[16] Lautens, M.; Crudden, C. M. Scope of the Cobalt-Catalyzed [2+2+2] Homo-Diels-Alder reaction. *Organometallics* **1989**, *8*(11), 2733–2735.
[17] (a) Yang, J.; Seto, Y. W.; Yoshikai, N. Cobalt-Catalyzed Intermolecular Hydroacylation of Olefins Through Chelation-Assisted Imidoyl C–H Activation. *ACS Catal.* **2015**, *5*(5), 3054–3057. (b) Yang, J.; Rérat, A.; Lim, Y. J.; Gosmini, C.; Yoshikai, N. Cobalt-Catalyzed Enantio- and Diastereoselective Intramolecular Hydroacylation of Trisubstituted Alkenes. *Angew. Chem. Int. Ed.* **2017**, *56*(9), 2449–2453. (c) Chen, Q.-A.; Kim, D. K.; Dong, V. M. Regioselective Hydroacylation of 1,3-Dienes by Cobalt Catalysis. *J. Am. Chem. Soc.* **2014**, *136*(10), 3772–3775.
[18] (a) Sang, H. L.; Yu, S.; Ge, S. Cobalt-Catalyzed Regioselective Stereoconvergent Markovnikov 1,2-Hydrosilylation of Conjugated Dienes. *Chem. Sci.* **2018**, *9*, 973–978. (b) Kim, Y. B.; Kim, D.; Dighe, S. U.; Chang, S.; Park, J.-W. Cobalt-Hydride Catalyzed Hydrosilylation of 3-Alkynes Accompanying π-Bond Migration. *ACS Catal.* **2021**, *11*(3), 1548–1553.
[19] Crépy, K. V. L.; Imamoto, T. Recent Developments in Catalytic Asymmetric Hydrogenation Employing P-Chirogenic Diphosphine Ligands. *Adv. Synth. Catal.* **2003**, *345*, 79–101.
[20] Chan, A. S. C.; Pluth, J. J.; Halpern, J. Intermediates in Homogeneous Catalytic Hydrogenation. The Crystal and Molecular Structure of the Methyl(Z)-*α*-acetamidocinnamate Adduct of 1,2-Bis(diphenylphosphino)ethanerhodium(I). *Inorganic Chim. Acta* **1979**, *37*, L477–L479.
[21] Chua, P. S.; Roberts, N. K.; Bosnich, B.; Okrasinski, S. J.; Halpern, J. The Origins of the Enantioselection in Asymmetric Catalytic

Hydrogenation of Amino-Acid Precursors. *J. C. S. Chem. Comm.* **1981**, *937*, 1278-1280.
[22] Chan, A. S. C.; Pluth, J. J.; Halpern, J. Identification of the Enantioselective Step in the Asymmetric Catalytic Hydrogenation of a Prochiral Olefin. *J. Am. Chem. Soc.* **1980**, *102*(18), 5952–5954.
[23] Chan, A. S. C.; Halpern, J. Interception and Characterization of a Hydridoalkylrhodium Intermediate in a Homogeneous Catalytic Hydrogenation Reaction. *J. Am. Chem. Soc.* **1980**, *102*(2), 838–840.
[24] McCulloch, B.; Halpern, J. Catalyst-Substrate Adducts in Asymmetric Catalytic Hydrogenation. Crystal and Molecular Structure of [((*R*,*R*)-1,2-Bis{phenyl-*o*-anisoylphosphino}ethane)(methyl(*Z*)-β-propyl-α-acetamidoacrylate)]rhodium Tetrafluoroborate, [Rh(DIPAMP)(MPAA)]BF_4. *Organometallics* **1990**, *9*(5), 1392–1395.
[25] Landis, C. R.; Halpern, J. Asymmetric Hydrogenation of Methyl-(Z)-α-acetamidocinnamate Catalyzed by {1,2-Bis((phenyl-*o*-anisoyl)phosphino)ethane}rhodium(I): Kinetics, Mechanism, and Origin of Enantioselection. *J. Am. Chem. Soc.* **1987**, *109*(6), 1746–1754.
[26] Halpern, J. Mechanism of Stereoselectivity of Asymmetric Hydrogenation. *Science* **1982**, *217*(4558), 401–407.
[27] Gridnev, I. D.; Higashi, N.; Asakura, K.; Imamoto, T. Mechanism of Asymmetric Hydrogenation Catalyzed by a Rhodium Complex of (*S*,*S*)-1,2-Bis(*tert*-butylmethylphosphino)ethane. Dihydride Mechanism of Asymmetric Hydrogenation. *J. Am. Chem. Soc.* **2000**, *122*, 7183–7194.
[28] Gridnev, I. D.; Higashi, N.; Imamoto, T. On the Origin of Opposite Stereoselection in the Asymmetric Hydrogenation of Phenyl- and *tert*-Butyl-substituted Enamides. *J. Am. Chem. Soc.* **2000**, *122*, 10486–10487.
[29] Gridnev, I. D.; Higashi, N.; Imamoto, T. Formation of a Stable Rhodium(I) Dihydride Complex and its Reactions with Prochiral Substrates of Asymmetric Hydrogenation. *Organometallics* **2001**, *20*, 4542–4553.
[30] Gridnev, I. D.; Yasutake, M.; Higashi, N.; Imamoto, T. Asymmetric Hydrogenation of Enamides with Rh-BisP* and Rh-MiniPhos Catalysts. Scope, Limitations, and Mechanism. *J. Am. Chem. Soc.* **2001**, *123*, 5268–5276.
[31] Gridnev, I. D.; Imamoto, T. Reaction of a Rhodium-MiniPhos Complex with Dihydrogen: NMR and Computational Study. *Organometallics* **2001**, *20*, 545–549.
[32] Gridnev, I. D.; Imamoto, T. On the Mechanism of Stereoselection in Rh-Catalyzed Asymmetric Hydrogenation: A General Approach for Predicting the Sense of Enantioselectivity. *Acc. Chem. Res.* **2004**, *37*(9), 633–644.
[33] Imamoto, T.; Yashio, K.; Crépy, K. V. L.; Katagiri, K.; Takahashi, H.; Kouchi, M.; Gridnev, I. *P*-Chiral Tetraphosphine Dirhodium Complex as a Catalyst for Asymmetric Hydrogenation: Synthesis, Structure, Enantioselectivity, and Mechanism. Stereoselective Formation of a Dirhodium Tetrahydride Complex and its Reaction with Methyl-(*Z*)-α-acetamidocinnamate. *Organometallics* **2006**, *25*, 908–914.
[34] Gridnev, I. D.; Imamoto, T.; Hoge, G.; Kouchi, M.; Takahashi, H. Asymmetric Hydrogenation Catalyzed by a Rhodium Complex of (*R*)-(*tert*-Butylmethylphosphino)(di-*tert*-butylphosphino)methane: Scope of Enantioselectivity and Mechanistic Study. *J. Am. Chem. Soc.* **2008**, *130*, 2560–2572.
[35] Gridnev, I. D.; Imamoto, T. Mechanism of Enantioselection in Rh-Catalyzed Asymmetric Hydrogenation. The Origin of Utmost Catalytic Performance. *Chem. Commun.* **2009**, 7447–7464.
[36] Gridnev, I. D.; Imamoto, T. Challenging the Major/Minor Concept in Rh-Catalyzed Asymmetric Hydrogenation. *ACS Catal.* **2015**, *5*, 2911–2915.
[37] Brown, J. M.; Chaloner, P. A. Structural Characterization of a Transient Intermediate in Rhodium-Catalyzed Asymmetric Homogeneous Hydrogenation. *J. C. S. Chem. Commun.* **1980**, 344–346.
[38] Brown, J. M.; Chaloner, P. A. The Mechanism of Asymmetric Homogeneous Hydrogenation. Rhodium(I) Complexes of Dehydroamino Acids Containing Asymmetric Ligands Related to Bis(1,2-diphenylphosphino)ethane. *J. Am. Chem. Soc.* **1980**, *102*(9), 3040–3048.
[39] Brown, J. M.; Chaloner, P. A.; Glaser, R.; Geresh, S. Intermediates in Asymmetric Hydrogenation: The Structure and ^{31}P NMR Spectra of Rhodium Enamide Complexes Containing 1*R*,2*R*-*trans*-1,2-*Bis*(diphenylphosphinomethyl)cyclobutene. *Tetrahedron* **1980**, *36*, 815–825.
[40] Brown, J. M.; Chaloner, P. A.; Kent, A. G.; Murrer, B. A.; Nicholson, P. N.; Parker, D.; Sidebottom, P. J. The Mechanism of Asymmetric Homogeneous Hydrogenation, Solvent Complexes and Dihydrides from Rhodium Diphosphite Precursors. *J. Organomet. Chem.* **1981**, *216*, 263–276.
[41] Brown, J. M.; Parker, D. Mechanism of Asymmetric Homogeneous Hydrogenation. Rhodium-Catalyzed Reductions with Deuterium and Hydrogen Deuteride. *Organometallics* **1982**, *1*, 950–956.
[42] Armstrong, S. K.; Brown, J. M. The Stereochemistry of Enamide Intermediates in DuPhos-Rh(I) Catalyzed Asymmetric Hydrogenation. *Tet. Lett.* **1993**, *34*(5) 879–882.
[43] Ramsden, J. A.; Claridge, T. D. W.; Brown, J. M. Structure and Dynamics of Intermediates in Asymmetric Hydrogenation by Rhodium Complexes of (2-Methoxyphenyl)-*P*-phenyl-*P*-[2'-diphenylphosphino]ethylphosphine. *J. Chem. Soc., Chem. Commun.* **1995**, 2469–2471.
[44] Evans, D. F. The Determination of the Paramagnetic Susceptibility of Substances in Solution by Nuclear Magnetic Resonance. *J. Chem. Soc.* **1959**, *2003–2005*.
[45] Halpern, J. Mechanism of Stereoselectivity of Asymmetric Hydrogenation. *Science* **1982**, *217*, 401–407.
[46] Bircher, H.; Bender, B. R.; Philipsborn, W. v. Interconversion of Diastereomeric Complexes Involved in Rh(I)-Catalyzed Asymmetric Hydrogenation: a (^{31}P,^{31}P) EXSY NMR Study. *Mag. Res. Chem.* **1993**, *31* 293–298.
[47] Zhong, H.; Beromi, M. M.; Chirik, P. J. Ligand Substitution and Electronic Strucutre Studies of Bis(phosphine)cobalt Cyclooctadiene Precatalysts for Alkene Hydrogenation. *Can. J. Chem.* **2020**, *99*, 193–201.
[48] Pauling, L. Metal-Metal Bond Lengths in Complexes of Transition Metals. *Proc. Natl. Acad. Sci. U. S. A.* **1976**, *73*, 4290–4293.
[49] Fryzuk, M. D.; Ng, J. B.; Rettig, S. J.; Huffman, J. C.; Jonas, K. Nature of the Catalytically Inactive Cobalt Hydride Formed Upon Hydrogenation of Aromatic Substrates. Structure and Characterization of the Binuclear Cobalt Hydride $[\{^{i}Pr_2P(CH_2)_3P^{i}Pr_2\}Co]_2(H)(\mu\text{-}H)_3$, *Inorg. Chem.* **1991**, *30*, 2437–2441.
[50] Gray, M.; Hines, M. T.; Parsutkar, M. M.; Wahlstrom, A. J.; Brunelli, N. A.; RajanBabu, T. V. Mechanism of Cobalt-Catalyzed Heterodimerization of Acrylates and 1,3-Dienes. A Potential Role of Cationic Cobalt(I) Intermediates. *ACS Catal.* **2020**, *10*, 4337–4348.
[51] Saper, N. I.; Hartwig, J. F. Mechanistic Investigations of the Hydrogenolysis of Diaryl Ethers Catalyzed By Nickel Complexes of *N*-Heterocyclic Carbene Ligands. *J. Am. Chem. Soc.* **2017**, *139*, 17667–17676.
[52] Sun, Y.; Landau, R. N.; Wang, J.; LeBlond, C.; Blackmond, D. G. A Re-Examination of Pressure Effects on Enantioselectivity in Asymmetric Catalytic Hydrogenation. *J. Am. Chem. Soc.* **1996**, *118*, 1348–1353.
[53] Burés, J. Variable Time Normalization Analysis: General Graphical Elucidation of Reaction orders from Concentration Profiles. *Angew. Chem. Int. Ed.* **2016**, *55* 16084–16087.
[54] Landis, C. R.; Brauch, T. W. Probing the Nature of H_2 Activation in Catalytic Asymmetric Hydrogenation. *Inorganica Chim. Acta* **1998**, *270*, 285–297.
[55] (a) Hopmann, K. H.; Bayer, A. On the Mechanism of Iridium-Catalyzed Asymmetric Hydrogenation of Imines and Alkenes: A Theoretical Study. *Organometallics* **2011**, *30*(9), 2483–2497. (b) Tutkowski, B.; Kerdphon, S.; Limé, E.; Helquist, P.; Andersson, P. G.; Wiest, O.; Norrby, P.-O., Revisiting the Stereodetermining Step

in Enantioselective Iridium-Catalyzed Imine Hydrogenation. *ACS Catal.* **2018**, *8*(1), 615–623.
[56] Morello, G. R.; Zhong, H.; Chirik, P. J.; Hopmann, K. H. Cobalt-Catalyzed Alkene Hydrogenation: a Metallacycle Can Explain the Hydroxyl Activating Effect and the Diastereoselectivity. *Chem. Sci.* **2018**, *9*(22), 4977–4982.
[57] Pavlovic, Lj. (2020) *Towards Enantioselective Carboxylation and Hydrogenation Reactions: Quantum Chemical Modelling of Homogeneous Reactions (Doctoral Thesis)*, https://munin.uit.no/handle/10037/18943.
[58] Pavlovic, Lj.; Mendelsohn, L.; Zhong, H.; Chirik, P.; Hopmann, K. H. Asymmetric Cobalt-Catalyzed Hydrogenation of Enamides: Insights into Mechanisms and Solvent Effects, *Organometallics*, (DOI: 10.1021/acs.organomet.2c00180).
[59] Ryu, H.; Park, J.; Kim, H. K.; Park, J. Y.; Kim, S.-T.; Baik, M.-H., Pitfalls in Computational Modeling of Chemical Reactions and How to Avoid Them. *Organometallics* **2018**, *37*(19), 3228–3239.

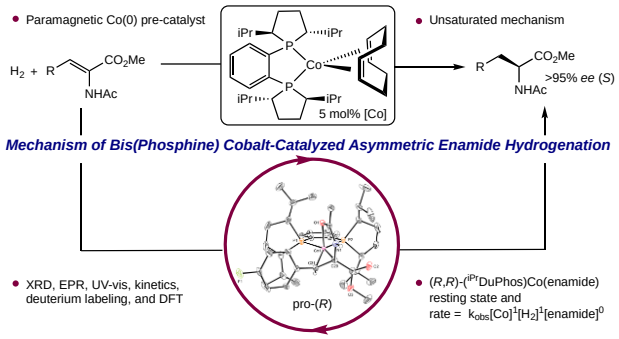
Paramagnetic Co(0) pre-catalyst
H2 + R
CO2Me
NHAc
iPr
iPr
P
Co
P
iPr
iPr
5 mol% [Co]
Unsaturated mechanism
R
CO2Me
NHAc
>95% ee (S)
Mechanism of Bis(Phosphine) Cobalt-Catalyzed Asymmetric Enamide Hydrogenation
XRD, EPR, UV-vis, kinetics, deuterium labeling, and DFT
pro-(R)
(R,R)-(iPrDuPhos)Co(enamide) resting state and
rate = kobs[Co]1[H2]1[enamide]0